Letters

Exact Solution of ZVS Boundaries and AC-Port Currents in Dual Active Bridge Type DC–DC Converters

Suyash Sushilkumar Shah, *Student Member, IEEE*, Vishnu Mahadeva Iyer, *Student Member, IEEE*, and Subhashish Bhattacharya, *Senior Member, IEEE*

***Abstract*—This letter presents an approach to develop an exact, unified model of zero voltage switching (ZVS) regions and ac-port currents (peak and RMS) in dual active bridge type dc–dc converters for all its operating modes and modulation strategies. It is executed for a single-phase system, where the method is used to compute closed-form expressions of ac current at switching instants. Then, exact formulae of ZVS regions for all devices, system peak, and RMS currents are derived. Simulation and hardware results for forward and reverse power transfer are reported to validate the proposed approach.**

***Index Terms*—AC current, bidirectional dc–dc converter, dual active bridge (DAB), modeling, peak current, RMS current, soft switching, zero voltage switching (ZVS), ZVS boundaries.**

I. Introduction

THE dual active bridge (DAB) type converters are a class of bidirectional isolated dc–dc systems introduced in [1] and [2]. This class of converter systems is popular for high-power applications such as electric vehicle charging [3]. Its single phase form, as shown in Fig. 1(a), comprises of two full-bridge converter circuits generating square or quasi-square wave ac voltages across a transformer-inductor arrangement.

The operation of a DAB converter is characterized by the duty ratios (d_1 and d_2) of the square or quasi-square wave ac voltages and the phase shift (ϕ) between them, as shown in Fig. 1(b). The simplest operating mode is single phase shift (SPS) modulation, where the ac voltages are square wave in nature. Advanced modulation schemes, including extended phase shift (EPS), double phase shift (DPS), and triple phase shift (TPS), generate quasi-square-wave voltages at either or both ac ports [4].

A key advantage of using DAB converters is its soft-switched turn-ON capability for all its semiconductor devices [2]. It eliminates the turn-ON losses and improves efficiency. However, the ideal operating range where zero voltage switching (ZVS) turn-ON may be achieved is limited by system parameters and its operating conditions [2]. It is, therefore, essential to understand the boundaries of the region where ZVS turn-ON is maintained.

Manuscript received October 26, 2018; accepted November 23, 2018. Date of publication November 30, 2018; date of current version April 20, 2019. *(Corresponding author: Suyash Sushilkumar Shah.)*

The authors are with the NSF FREEDM Systems Engineering Research Center, North Carolina State University, Raleigh, NC 27606 USA (e-mail:

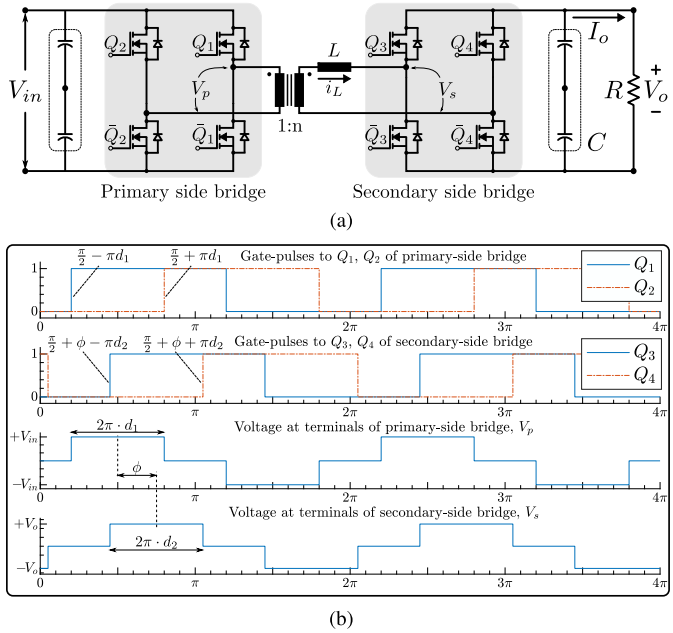

Fig. 1. (a) Circuit topology of a single-phase DAB converter. (b) Timing diagram of the converter characterized by ϕ, d_1, d_2.

Several papers report the analytic models describing the ZVS boundaries and ac-port currents of a DAB converter operating in simple phase-shift modulation [2] and its more complex modes [5], [6]. Most papers are limited to a specific modulation strategy and restricted operating range [5]. In others, multiple submodes are identified resulting in disjointed and mode-dependent description of ZVS regions [6]. Some papers [7] present unified models in form of infinite series, thereby requiring a tradeoff between accuracy and complexity.

In this letter, an approach is developed for an exact, unified model identifying ZVS regions, peak, and RMS currents in DAB type dc–dc converters for any operating mode or modulation strategy. These are derived from switching instant currents that are modeled based on the principle of superposition. The method is realized for a single-phase system.

II. Basis of the Proposed Approach

The superposition principle is the basis of state space averaged modeling of power electronic converters [8]. Its variant has been

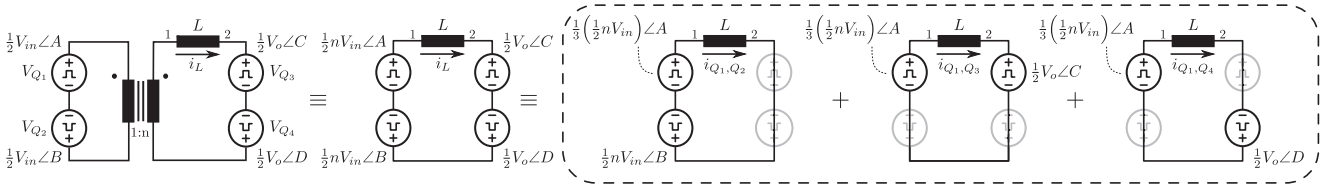

Fig. 2. Model of a DAB converter to compute currents (I_{Q_1} and $-I_{Q_1}$) through $\{Q_1, \bar{Q}_1\}$ at their turn-ON (referred to the secondary side).

TABLE I
VOLTAGE SIGNALS GENERATED BY Q_1, Q_2, Q_3, AND Q_4

Voltage signals	Phase-shift with respect to				
	$t=0$	V_{Q_1}	V_{Q_2}	V_{Q_3}	V_{Q_4}
V_{Q1}	A	0	$A-B$	$A-C$	$A-(D-\pi)$
V_{Q2}	B	$B-A$	0	$(B-\pi)-C$	$B-D$
V_{Q3}	C	$C-A$	$C-(B-\pi)$	0	$C-D$
V_{Q4}	D	$(D-\pi)-A$	$D-B$	$D-C$	0

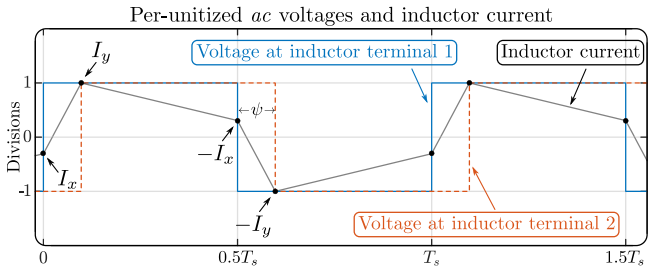

Fig. 3. Typical waveform for sub-circuits in Fig. 2.

employed for modeling of a DAB converter across its operating modes and modulation strategies in [4]. However, it is a reduced-order model and, therefore, cannot describe ZVS boundaries or ac-port currents of the converter.

In a DAB converter, the square or quasi-square wave ac voltage waveform is generated by appropriate switching of its four constituent half-bridge legs (Q_1, Q_2, Q_3, and Q_4). These legs generate full square-wave ac voltage signals, $\{V_{Q_1}, V_{Q_2}, V_{Q_3}, V_{Q_4}\}$, which are phase shifted from one another by appropriate angles, as shown in Fig. 1(b) and summarized in Table I. A factor of one-half appears in the voltages as these are referred to the respective dc-port capacitor midpoint. A schematic of the converter ac port in terms of four ac voltage sources and their respective phase-shift angles is illustrated in Fig. 2. The variables A, B, C, and D are defined in the following, using Fig. 1(b)

$$A = \frac{\pi}{2} - \pi d_1; \quad B = \frac{\pi}{2} + \pi d_1$$
$$C = \frac{\pi}{2} + \phi - \pi d_2; \quad D = \frac{\pi}{2} + \phi + \pi d_2. \tag{1}$$

The circuit in Fig. 2 can be analyzed in multiple ways using the principle of superposition. Consider two voltage sources ($nV_{\text{in}}/2$ and $V_o/2$) with other sources shorted. If ψ is an arbitrary phase-shift angle between them, then $\{I_x, I_y\}$ are inductor current magnitudes at the rising edges of those sources, as shown by representative waveforms in Fig. 3 and expressed as following:

$$I_x = -\frac{1}{4}\frac{nV_{\text{in}}}{\omega L}\left(\pi - M\cdot(\pi - 2|\psi|)\right)$$
$$I_y = +\frac{1}{4}\frac{nV_{\text{in}}}{\omega L}\left(M\pi - (\pi - 2|\psi|)\right) \tag{2}$$

where, $M = \frac{V_o}{nV_{\text{in}}}$.

III. AC PORT MODEL

Without loss of generality, the half-bridge leg Q_1 formed by complementary switches, $\{Q_1, \bar{Q}_1\}$, assumes the role of reference phase with respect to which the phase-shift angles of voltages generated by other half-legs (Q_2, Q_3, and Q_4) are described. In effect, the converter operation is decomposed into

TABLE II
AC-PORT OR TRANSFORMER CURRENT AT TURN-ON INSTANTS OF Q_1, Q_2, Q_3, AND Q_4, REFERRED TO ITS SECONDARY SIDE

Current	Expressions $\left(K = \frac{1}{2}\frac{nV_{in}}{\omega L}\right)$
I_{Q_1}	$+K\cdot\left[M\left(\pi - \lvert C-A\rvert - \lvert D-\pi-A\rvert\right) - \lvert B-A\rvert\right]$
I_{Q_2}	$-K\cdot\left[M\left(\pi - \lvert D-B\rvert - \lvert C-B+\pi\rvert\right) - \lvert B-A\rvert\right]$
I_{Q_3}	$-K\cdot\left[\pi - \lvert C-A\rvert - \lvert C-B+\pi\rvert - M\lvert D-C\rvert\right]$
I_{Q_4}	$+K\cdot\left[\pi - \lvert D-B\rvert - \lvert D-\pi-A\rvert - M\lvert D-C\rvert\right]$

three circuits formed by $\{Q_1, Q_2\}, \{Q_1, Q_3\}$, and $\{Q_1, Q_4\}$, referred to the secondary side. Each circuit comprises of two square-wave ac voltages separated by a phase-shift angle (see Table I). The equivalent sub-circuits are shown in Fig. 2. A factor of one-third appears in V_{Q_1}, as it is distributed among the sub-circuits. In each sub-circuit, the current at the rising edge of V_{Q_1}—referred to the secondary side of the transformer—is expressed in the following, derived using (2):

$$I_{x,Q_1,Q_2} = -\frac{1}{4}\frac{nV_{\text{in}}}{\omega L}\left(\frac{\pi}{3} - [\pi - 2|B-A|]\right)$$
$$I_{x,Q_1,Q_3} = -\frac{1}{4}\frac{nV_{\text{in}}}{\omega L}\left(\frac{\pi}{3} - M\cdot[\pi - 2|C-A|]\right)$$
$$I_{x,Q_1,Q_4} = -\frac{1}{4}\frac{nV_{\text{in}}}{\omega L}\left(\frac{\pi}{3} - M\cdot[\pi - 2|D-\pi-A|]\right). \tag{3}$$

Half-leg Q_1 is the common reference. Therefore, the currents in (3) are simply added to obtain total transformer current—referred to its secondary side—at the turn-ON instant of Q_1.

$$I_{Q_1} = \left(I_{x,Q_1,Q_2} + I_{x,Q_1,Q_3} + I_{x,Q_1,Q_4}\right). \tag{4}$$

Its polarity is in direct correlation to whether the complementary switches $\{Q_1, \bar{Q}_1\}$ turn-ON with zero voltage. In a similar approach, the ac port or transformer current at the turn-ON instants of other semiconductor devices are explicitly calculated and summarized in Table II.

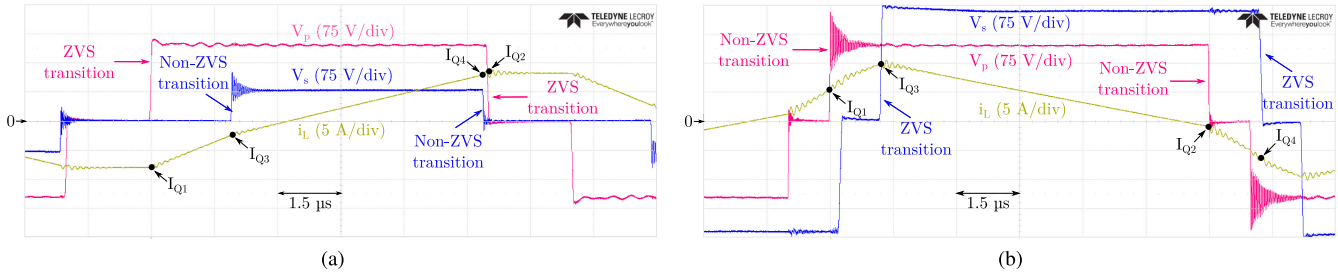

Fig. 4. Experimental results demonstrating ZVS turn-ON on (a) primary-side and (b) secondary-side semiconductor devices.

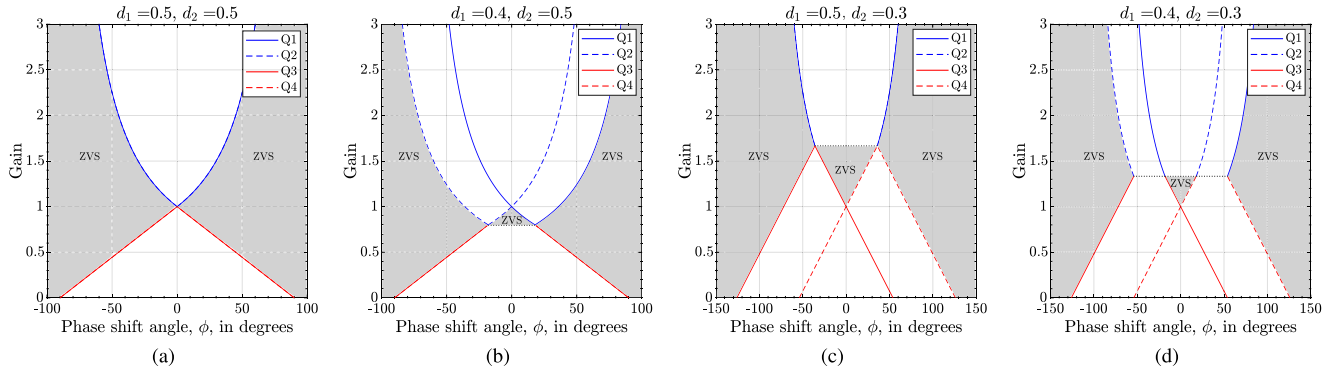

Fig. 5. ZVS regions and boundaries for (a) phase-shift modulation, (b) duty-ratio modulation for primary-side bridge, (c) secondary-side bridge, and (d) both bridges. Shaded region indicates soft-switched turn-ON for all semiconductor devices.

A. Determination of ZVS Regions and Boundaries

In ideal conditions, the semiconductor device turns-ON at zero voltage when the current flows through its anti-parallel diode before commuting to the device. An example is illustrated in Fig. 4. In Fig. 4(a), $I_{Q_1} < 0$ and $I_{Q_2} > 0$; therefore, primary-side devices are soft switched. Similarly, in Fig. 4(b), $I_{Q_3} > 0, I_{Q_4} < 0$ and thus, secondary-side devices turn-ON at zero voltage. The hard switched turn-ON of semiconductor devices is accompanied by losses and ringing in the voltage waveform; it appears due to sudden discharge of the output parasitic capacitance of the device. The ZVS regions and boundaries may, therefore, be calculated using the following:

$$I_{Q_1}, I_{Q_4} \leq 0\,; \quad I_{Q_2}, I_{Q_3} \geq 0. \tag{5}$$

The exact solution to the boundaries of ZVS regions for each converter leg is expressed in the following set of equations:

$$\begin{aligned}
&\text{For } \{Q_1, \bar{Q}_1\} : M \leq \frac{|B-A|}{\pi - |C-A| - |D-\pi-A|}\\
&\text{For } \{Q_2, \bar{Q}_2\} : M \leq \frac{|B-A|}{\pi - |C-B+\pi| - |D-B|}\\
&\text{For } \{Q_3, \bar{Q}_3\} : M \geq \frac{\pi - |C-A| - |C-B+\pi|}{|D-C|}\\
&\text{For } \{Q_4, \bar{Q}_4\} : M \geq \frac{\pi - |D-\pi-A| - |D-B|}{|D-C|}.
\end{aligned} \tag{6}$$

The ZVS regions and boundaries are illustrated for SPS [see Fig. 5(a)], EPS/DPS [see Fig. 5(b) and (c)], and TPS [see Fig. 5(d)] modulation strategies.

B. Calculation of RMS and Peak AC Currents

The ac current waveform of a DAB converter is of half-wave symmetric, piecewise linear nature, i.e., its peak and RMS values can be calculated if the vertices of each piecewise linear element in one-half cycle are known.

1) Consider ac-port currents $I_{Q_1}, I_{Q_2}, I_{Q_3}$, and I_{Q_4} as expressed in Table II.
2) Consider a half-cycle from the minimum of angles, A, B, C, and D; identify the switching events. If the angle is within 180° of minimum, the corresponding high-side device turns-ON at t_{Q_x} with current I_{Q_x}; else, it turns-OFF at t_{Q_x} with $-I_{Q_x}$, i.e.

$$t_{Q_x} = \begin{cases} \frac{\theta}{2\pi} T_s, & \text{if } \theta \leq \min(A,B,C,D) + \pi \\ \frac{\theta-\pi}{2\pi} T_s, & \text{if } \theta > \min(A,B,C,D) + \pi \end{cases}$$
$$\forall\ \theta \in \{A,B,C,D\} \quad \text{and} \quad \forall \quad x \in \{1,2,3,4\}. \tag{7}$$

3) Sort the switching events in chronological order to find vertices of piecewise linear waveform of ac current, i.e.

$$\{I_{t_1}, I_{t_2}, I_{t_3}, I_{t_4}\} \in \{\pm I_{Q_1}, \pm I_{Q_2}, \pm I_{Q_3}, \pm I_{Q_4}\} \text{ at } \{t_1, t_2, t_3, t_4\} \in \{t_{Q_1}, t_{Q_2}, t_{Q_3}, t_{Q_4}\}. \tag{8}$$

4) Compute RMS value of each piecewise linear element, as in (9). Compute the total RMS current, as in (10)

$$I_{\text{RMS},k} = \sqrt{\frac{2}{3}\left(I_{t_{k+1}}^2 + I_{t_k}^2 + I_{t_{k+1}} I_{t_k}\right)\frac{t_{k+1}-t_k}{T_s}}$$
$$\forall\ k \in \{1,2,3,4\};\ \ I_{t_5} = -I_{t_1};\ \ t_5 = t_1 + 0.5T_s \tag{9}$$

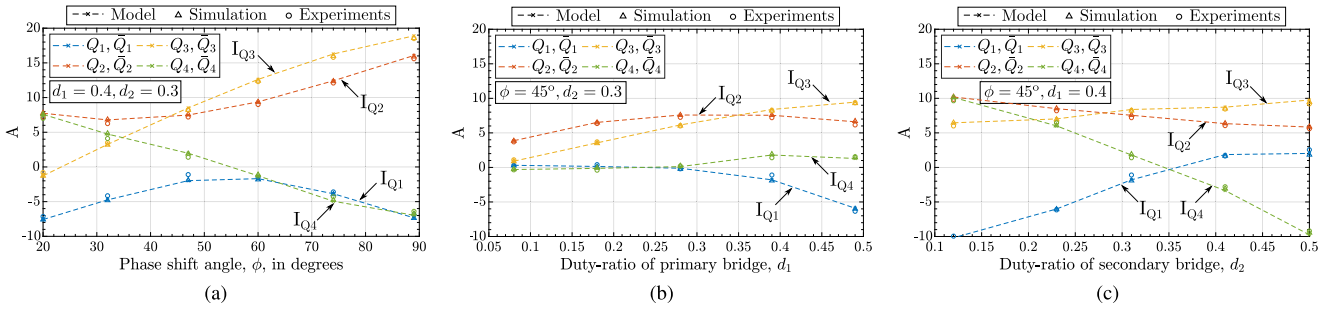

Fig. 6. Forward power transfer: Comparison of simulation and experimental results with the model for ac-port currents at switching instants. (a) With phase-shift angle ϕ. (b) With duty ratio of primary side bridge d_1. (c) With duty ratio of secondary-side bridge d_2.

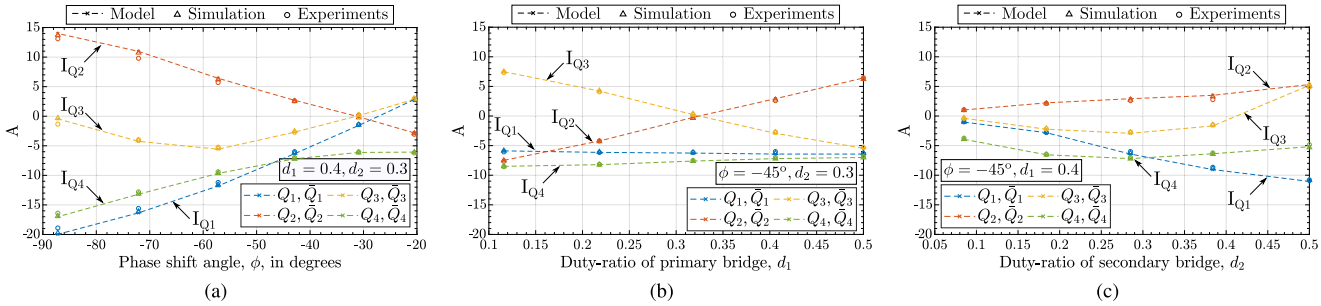

Fig. 7. Reverse power transfer: Comparison of simulation and experimental results with the model for ac-port currents at switching instants. (a) With phase-shift angle ϕ. (b) With duty ratio of primary side bridge d_1. (c) With duty ratio of secondary-side bridge d_2.

TABLE III
SYSTEM PARAMETERS

Parameter	Variable	Value
Input DC voltage	V_{in}	200 V
Switching frequency	f_s	50 kHz
Power transfer inductance	L	67 μH
Output load	R, C	50 Ω, 450 μF

$$I_{\text{RMS, pri}} = n \cdot I_{\text{RMS, sec}} = n \cdot \left(\sum_{k=1}^{4} I_{\text{RMS},k}^2 \right)^{1/2}. \quad (10)$$

Similarly, as the vertices of each piecewise linear element in the half-cycle are known, the peak current flowing through the transformer and semiconductor devices may simply be expressed as in the following:

$$I_{pk,\text{pri}} = n \cdot I_{pk,\text{sec}} = n \cdot \max\left(|I_{Q_1}|, |I_{Q_2}|, |I_{Q_3}|, |I_{Q_4}|\right). \quad (11)$$

IV. EXPERIMENTS AND RESULTS

The experiments are conducted on a hardware prototype, parameters of which are listed in Table III. The transformer turns ratio, n, is unity. The ac-port current at the turn-ON instants of semiconductor devices ($I_{Q_1}, I_{Q_2}, I_{Q_3}$, and I_{Q_4}) for forward and reverse power transfer are illustrated in Figs. 6 and 7, respectively. One of the three control variables, $\{\phi, d_1, d_2\}$, varies, whereas the other two remain constant. The simulation and experimental results are in agreement with those extracted from the model. The ac port or transformer RMS current model, (7)–(10), is similarly validated for forward and reverse power transfer in Fig. 8.

V. DISCUSSION

The exact, unified, closed-form solution of ZVS boundaries for a single-phase DAB converter in any operating mode and modulation strategy is derived in (6). It is evident that ZVS regions are dependent only on the voltage gain, M, and the respective phase-shift angles (A, B, C, and D) of four constituent half-bridge legs (Q_1, Q_2, Q_3, and Q_4).

In general, there are four points of intersection between the ZVS boundaries of primary and secondary-side converter legs, listed in the following equation. The gain-axis coordinate, M, of these points is the ratio d_1/d_2 [7], as shown in Fig. 5. The x-axis coordinates, ϕ, are computed by substituting M in (6) by d_1/d_2 and solving the boundary condition, to get the following:

$$(\phi, M) = \begin{cases} \left(\pm\pi(d_1 - d_2), \frac{d_1}{d_2}\right) \\ \left(\pm\pi(1 - d_1 - d_2), \frac{d_1}{d_2}\right). \end{cases} \quad (12)$$

The ZVS boundaries of $\{Q_1, Q_2\}$ intersect with those of $\{Q_3, Q_4\}$ at single points. These points may coincide one another when either or both of d_1 or d_2 are one-half. Contrarily, the boundaries exhibit discontinuity between intersecting points when either d_1 or d_2 diverge from one-half [see Fig. 5(b)–(d)]; although practically, there is a boundary between those points, shown by the *black, dotted* line.

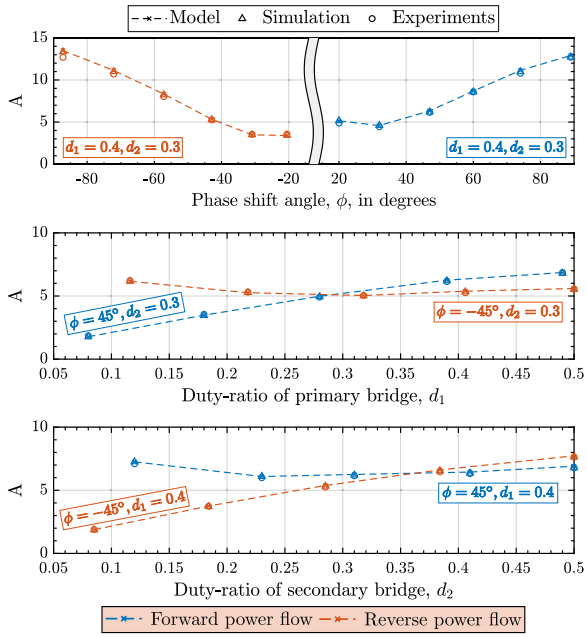

Fig. 8. Comparison of simulation and experimental results with the model for secondary-side RMS current ($I_{\text{RMS, sec}}$).

The exact, unified model of ac-port current at switching instants (see Table II), its peak (11), and RMS values (7)–(10) may be used to compute current ratings of semiconductor devices ($I_{\text{RMS, pri-sw}}$, $I_{\text{RMS, sec-sw}}$).

$$I_{\text{RMS, pri-sw}} = \frac{1}{\sqrt{2}} I_{\text{RMS, pri}}; \quad I_{\text{RMS, sec-sw}} = \frac{1}{\sqrt{2}} I_{\text{RMS, sec}}. \quad (13)$$

It may be used to estimate switching and conduction losses in the converter. It may also be used for design optimization encompassing all modes of a DAB converter, which is out of the scope of this letter.

VI. Conclusion

This letter proposes an approach, based on principle of superposition, to develop an exact model of ZVS boundaries and ac-port current in DAB type converters for all its operating modes and modulation strategies. Closed-form expressions of ac-port current at switching instants, its peak, and RMS values are derived. The ZVS boundary conditions are obtained to recognize the operating regions where soft switching is maintained. Simulation and experimental results are presented for forward and reverse power transfer operation of the converter; they are in agreement with those extracted from the model.

References

[1] R. W. D. Doncker, D. M. Divan, and M. H. Kheraluwala, "A three-phase soft-switched high power density DC/DC converter for high power applications," in *Proc. Conf. Rec. 1988 IEEE Ind. Appl. Soc. Annu. Meeting*, Oct. 1988, vol. 1, pp. 796–805.

[2] R. W. A. A. D. Doncker, D. M. Divan, and M. H. Kheraluwala, "A three-phase soft-switched high-power-density DC/DC converter for high-power applications," *IEEE Trans. Ind. Appl.*, vol. 27, no. 1, pp. 63–73, Jan./Feb. 1991.

[3] V. M. Iyer, S. Gulur, and S. Bhattacharya, "Small-signal stability assessment and active stabilization of a bidirectional battery charger," *IEEE Trans. Ind. Appl.*, vol. 55, no. 1, pp. 563–574, Jan.-Feb. 2019, doi: 10.1109/TIA.2018.2871101.

[4] S. S. Shah and S. Bhattacharya, "A simple unified model for generic operation of dual active bridge converter," *IEEE Trans. Ind. Electron.*, vol. 66, no. 5, pp. 3486–3495, May 2019.

[5] G. G. Oggier, G. O. Garćia, and A. R. Oliva, "Switching control strategy to minimize dual active bridge converter losses," *IEEE Trans. Power Electron.*, vol. 24, no. 7, pp. 1826–1838, Jul. 2009.

[6] J. Everts, "Closed-form solution for efficient ZVS modulation of DAB converters," *IEEE Trans. Power Electron.*, vol. 32, no. 10, pp. 7561–7576, Oct. 2017.

[7] J. Riedel, D. G. Holmes, B. P. McGrath, and C. Teixeira, "ZVS soft switching boundaries for dual active bridge DC–DC converters using frequency domain analysis," *IEEE Trans. Power Electron.*, vol. 32, no. 4, pp. 3166–3179, Apr. 2017.

[8] R. D. Middlebrook and S. Cuk, "A general unified approach to modelling switching-converter power stages," in *Proc. IEEE Power Electron. Spec. Conf.*, Jun. 1976, pp. 18–34.